IEEE Access
Multidisciplinary ⋮ Rapid Review ⋮ Open Access Journal

Received March 24, 2021, accepted April 11, 2021, date of publication April 16, 2021, date of current version April 26, 2021.

Digital Object Identifier 10.1109/ACCESS.2021.3073835

A Decoupling Network for Resonant and Non-Resonant Sub-1 GHz MIMO Mobile Terminal Antennas With Improved Compactness and Efficiency

WAI LOON CHEOR[1], (Graduate Student Member, IEEE), AZREMI ABDULLAH AL-HADI[1], (Senior Member, IEEE), PING JACK SOH[1], (Senior Member, IEEE), MOHD FAIZAL JAMLOS[2], (Senior Member, IEEE), AHMED MOHAMED ELSHIRKASI[1], XIAOMING CHEN[3], (Senior Member, IEEE), AND PRAYOOT AKKARAEKTHALIN[4], (Member, IEEE)

[1]Advanced Communication Engineering (ACE) Center of Excellence, Faculty of Electronic Engineering Technology, Universiti Malaysia Perlis, Arau 02600, Malaysia
[2]Faculty of Mechanical and Manufacturing Engineering, Universiti Malaysia Pahang, Pekan 26600, Malaysia
[3]Faculty of Electronic and Information Engineering, School of Information and Communications Engineering, Xi'an Jiaotong University, Xi'an 710049, China
[4]Department of Electrical and Computer Engineering, Faculty of Engineering, King Mongkut's University of Technology North Bangkok (KMUTNB), Bangkok 10800, Thailand

Corresponding authors: Azremi Abdullah Al-Hadi (azremi@unimap.edu.my) and Prayoot Akkaraekthalin (prayoot.a@eng.kmutnb.ac.th)

This work was supported in part by the Fundamental Research Grant Scheme (FRGS) through the Ministry of Education Malaysia under Grant FRGS/1/2019/TK04/UNIMAP/02/21, and in part by the King Mongkut's University of Technology North Bangkok under Grant KMUTNB-FF-65-21.

ABSTRACT In this work, the design procedure of a new decoupling network for different antennas is presented for mobile terminals operating in the Sub-1 GHz band (from 0.698 to 0.96 GHz). To evaluate its applicability for different resonant and non-resonant antenna types, two antenna elements have been chosen to be decoupled using the proposed decoupling network: a printed inverted-F antenna and a capacitive coupling element antenna. Simulation and measurement results showed that the decoupling network offer promising improvements in terms of impedance matching, port isolation, envelope correlation coefficient (ECC), and total efficiency. In addition, the antennas are also investigated with the ergodic capacity, multiplexing efficiency, gain, and diversity gain (both calculated using maximal ratio combining technique). Due to the contribution of the decoupling network, the ECC of both types of multiple antennas are less than 0.3, with a 30 % improvement in total efficiency and an inter-element spacing miniaturization of 34 %.

INDEX TERMS Decoupling networks, mutual coupling, multi-input multi-output, low frequency, mobile terminal antennas.

I. INTRODUCTION

The multi-input multi-output (MIMO) technology [1] is widely used in wireless communication systems to enhance channel capacity. The performance of a closely-spaced multiple antenna system is heavily dependent on the reduction of the strong coupling effects between its antenna elements. It is therefore challenging to design multiple-antenna system with a considerably compact size inside a mobile terminal chassis. In recent years, many researchers have adapted several methods to alleviate coupling effects [2]–[8]. Some of the common decoupling techniques are by implementing parasitic elements [2], [3], neutralization lines [4], defected ground structures [5], characteristic modes analysis [6], electromagnetic bandgap (EBG) structures [7], decoupling ground structures [8] and decoupling network [9]–[17].

In this paper, two types of antenna elements are proposed to evaluate the proposed decoupling network. The first is a resonant printed inverted-F antenna (PIFA), where the antenna element is matched and radiating at the desired frequency, whereas the second one is a non-resonant capacitive coupling element (CCE) antenna [18], [19]. These antennas are

The associate editor coordinating the review of this manuscript and approving it for publication was Luyu Zhao.

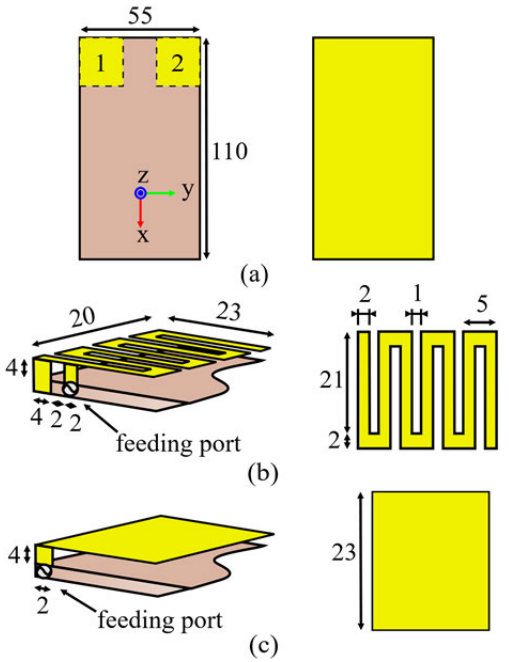

FIGURE 1. (a) Antenna locations studied in this work. Dimension of the (b) PIFA and (c) CCE antenna under study. All dimensions are in millimeter.

designed to operate in the Sub-1 GHz band, a band which is expected to remain relevant for future technologies [20]. This work is focused on the implementation of decoupling network on common mobile terminal antennas, i.e., PIFA and CCE which potentially can be further miniaturized [21], [22]. From the literature, such decoupling technique is mainly used in monopole antennas instead of PIFA and CCE [12]–[17], and are focused at decoupling antennas operating above 2.45 GHz [12], [13], [15]–[17]. On the contrary, the uniqueness of this work is that it is focused on decoupling PIFA and CCE antenna in the Sub-1 GHz band. Focused operation of mobile terminals in this band with narrower bandwidths allows the further wave propagation relative to higher frequency, besides minimizing the need for filtering components. The proposed antenna elements with the decoupling network are simulated and validated by measurements of the fabricated prototypes. The simulated and measured results are in a good agreement, with satisfactory reflection coefficients, isolation, envelope correlation coefficient (ECC) and total efficiency. Moreover, an excellent trade-off between mutual coupling and the inter-element distance is featured by the decoupling network, while achieving satisfactory total efficiency at the same time. These features are advantageous for mobile terminals operating with multiple non-resonant antennas at low frequencies. To the best of our knowledge, this is a pioneering work in decoupling of non-resonant antenna elements in the Sub-1 GHz band.

II. MULTI-ELEMENT ANTENNA

The antenna elements have been chosen to be positioned at the edge of the chassis based on [23], where the characteristic mode indicated in this area is most suited for multiple antennas operating frequency below 1 GHz. A chassis sized of 110 x 55 x 1.524 mm^3 is chosen to evaluate two types of antenna elements, as illustrated in Fig. 1(a). The PIFA is chosen to represent the resonant antenna, whereas the CCE antenna is selected to represent the non-resonant antenna elements. Both antenna types are located at the edge of the chassis and designed for Sub-1 GHz band operating from 0.698 to 0.960 GHz (with a center frequency, f_c of 0.829 GHz). The inter-element distance is 15 mm (0.08 λ_g) apart, which causes high coupling. All antenna elements are designed on a Rogers RO 4003C substrate with permittivity $\varepsilon_r = 3.38$. The design of the PIFA and CCE antenna elements are shown in Fig. 1(b) and 1(c), respectively. The overall size of both antenna elements is 20 mm x 23 mm^2. All the antennas are connected with a SMA connector as the feeding port. To enable a fair comparison, the CCE antennas are designed similarly in dimensions with the PIFA, and are located with an air gap of 4 mm above the chassis. On the other hand, the CCE antennas are matched using lumped components to enable its operation in the Sub-1 GHz band. The matching circuit is limited to two lumped elements to ensure design simplicity.

III. DESIGN PROCEDURE OF THE DECOUPLING NETWORK

The overall design flow for the decoupling network on the different types of multiple antennas is summarized in Fig. 2. Generally, the three main design stages in this work: i) the transmission line; ii) the decoupling network; and iii) the matching network are denoted in the dotted boxes in Fig. 3. The circuit of the decoupling network, Y_p is connected in parallel with the antennas, and consists of a reactive (X) and resistive (R) element. Finally, a simple L-section is applied as a matching circuit for frequency tuning. This procedure is applicable to both PIFAs and CCE antennas. A more specific design procedure is explained as follows. The mutual coupling between the elements is represented by the complex antenna admittance, $-Y_{21}$. A decoupling network with an admittance of Y_p can then applied in parallel to the antenna structure to eliminate the $-Y_{21}$, (so that $Y_p - Y_{21} = 0$). The antenna structure is assumed to be initially matched prior to the implementation of the decoupling network. Hence, the non-resonant CCE antennas are required to be matched using a pre-matching circuit. Next, a positive $R\{Y_{21}\}$ is required to be introduced to the antennas with an equivalent phase of $|\arg\{Y_{21}\}| \leq 90°$. The positive $R\{Y_{21}\}$ is introduced via an additional transmission line, with its length used to control the value of $\arg\{Y_{21}\}$ at a specific frequency. The combined implementation of a resistive element and a transmission line (instead of using the transmission line alone) adds to the design flexibility of the proposed decoupling network.

To estimate the values of the lumped element in the circuit of Y_p, the resistive and reactive elements can be calculated as follows:

$$R = \frac{1}{Re\{Y_{21}\}}$$

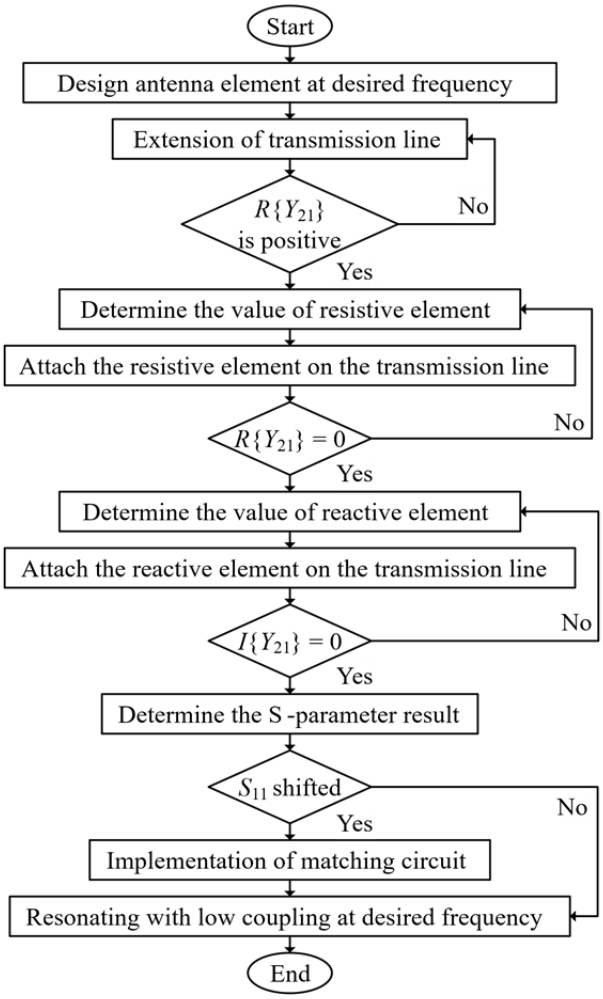

FIGURE 2. Design flow of the decoupling network and multiple antennas.

$$X = \frac{1}{Im\{Y_{21}\}} \tag{1}$$

These values are used to eliminate the real and imaginary parts of the $-Y_{21}$, respectively. For the reactive element, a capacitor or inductor can either be applied as X for a positive or negative susceptance at the specific frequency, respectively. The required value of the reactive element is estimated by:

$$X_C = \frac{1}{2\pi fC} \text{ and } X_L = 2\pi fL \tag{2}$$

It is known that resistive components connected to antenna feeds causes small amount of losses, and the rest of the power is ideally radiated by the antenna. However, an important point to consider is the original isolation between the two antenna elements, which the isolation prior to the implementation of the decoupling network. This factor directly affects the efficiency of the antenna, as low isolation results in lower efficiency. However, depending on the value of the resistor, this efficiency can be improved if the losses in the resistor

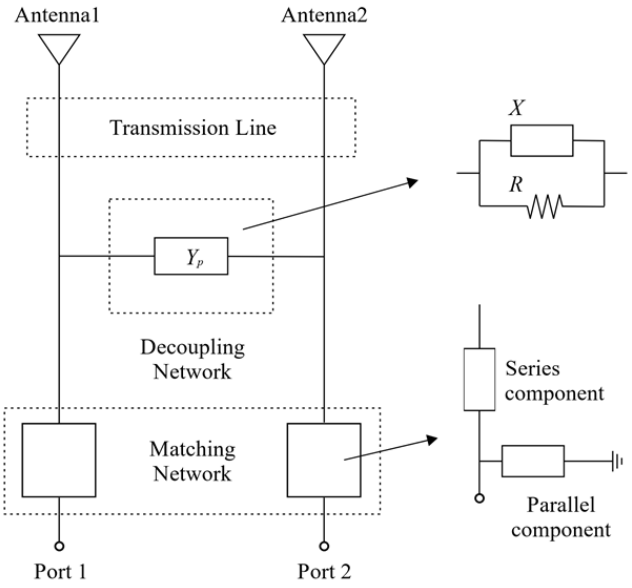

FIGURE 3. Schematic of the two-element antennas and the transmission line, the decoupling network and matching network.

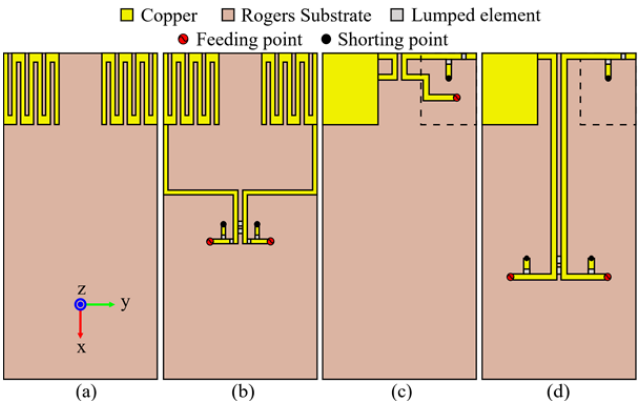

FIGURE 4. Layout of PIFA (a) without and (b) with the decoupling network; Layout of CCE antenna (c) without and (d) with the decoupling network.

is smaller than the improvement in isolation [13]. In other words, in this work, the power loss contributed by the resistors (499 Ω for the PIFA and 1024 Ω for the CCE) is small and negligible compared to the contribution of the decoupling network in preventing the coupling between the two ports of the antennas.

Fig. 4 depicts the layout of the PIFAs and CCE antennas with and without the decoupling network. The transmission line length of the for the PIFAs and CCE antennas is 75.5 mm (0.383 λ_g) and 72.48 mm (0.368 λ_g), respectively. Meanwhile, Table 1 summarizes the values of the lumped components in the circuit, including the pre-matching network components for the CCE antennas. For both the PIFA and CCE antenna designs, positive values are obtained for $Im\{Y_{21}\}$, and thus capacitors have been implemented as the reactive element in the decoupling network.

TABLE 1. Lumped component values for the fabricated prototypes.

Component	PIFA		CCE antenna	
Pre-Matching Network	-	-	Series Inductor	12 nH
	-	-	Parallel Capacitor	8.2 pF
Decoupling network	Resistor	499 Ω	Resistor	1024 Ω
	Capacitor	3.3 pF	Capacitor	1 pF
Matching network	Series Capacitor	100 pF	Series Inductor	10 nH
	Parallel Inductor	5.6 nH	Parallel Capacitor	1 pF

TABLE 2. Comparison of chassis size, decoupling size and inter-element distance between antennas.

Ref. (year)	Frequency	Chassis size	Size of antenna element	Size of decoupling element
[11]	2.6 GHz	0.97 x 3.055 λ_g	0.218 x 0.340 λ_g	0.17 x 0.22 λ_g
[13]	2.45 GHz	0.37 x 1.14 λ_g	0.360 x 0.025 λ_g	0.16 x 0.35 λ_g
[14]	0.74 GHz	0.46 x 0.72 λ_g	0.501 x 0.054 λ_g	0.5 x 0.08 λ_g
[17]	2.2 GHz	1.3 x 1.3 λ_g	0.857 x 0.765 λ_g	0.96 x 1.16 λ_g
[This work]	0.829 GHz	0.56 x 0.28 λ_g	0.116 x 0.101 λ_g	0.09 x 0.08 λ_g

Both antennas in this work are dimensioned at 23 x 20 mm^2 (0.116 x 0.1 λ_g). Table 2 summarizes the sizes of the chassis, antenna elements, and decoupling element in comparison with previous literature [11], [13], [14], [17]. It indicates that the proposed antenna element, which needs to theoretically be at least a quarter of a wavelength, can be designed on the smallest area compared to other works. Moreover, the area occupied by the decoupling element (0.09 x 0.08 λ_g) is also found to be the smallest among the existing literature.

IV. PERFORMANCE EVALUATION METRICS

In mobile terminal, the performance of the antennas is evaluated using the S-parameters. In addition, MIMO antenna and MIMO link metrics are implemented to further evaluate the performance of the MIMO antenna. In this work, the MIMO antenna metrics are first calculated (e.g., total efficiency and envelope correlation coefficient (ECC)). These parameters are then used to calculate the MIMO link metrics.

ECC is one of the essential metrics to determine the performance of MIMO antennas in a mobile terminal. It showed the correlation between the two antennas which are placed side-by-side in all combinations. MIMO antennas should have a low ECC value to ensure the antennas are uncorrelated and the threshold of the accepted value is 0.5 according to the literature [24]. The ECC, ρ_e in this work is evaluated from the antenna radiation patterns equation (3), as shown at the bottom of the next page, [25].

Meanwhile, the total efficiency (η_{tot}) in MIMO antenna is a function of the radiation efficiency (η_{rad}) and the matching efficiency ($\eta_{mis+coup}$). It includes the mutual coupling, as follows [26]:

$$\eta_{tot} = \eta_{rad}\eta_{(mis+coup)} = \eta_{rad}\left(1 - |S_{11}|^2 - |S_{12}|^2\right) \quad (4)$$

where parameters S_{11} and S_{12} indicate the mismatch loss and coupling loss between the MIMO antenna elements. Improved matching of these elements using the decoupling network can directly result in the improvement of total efficiency.

The ergodic capacity is defining as the rate of the achieved averaging capacity over the channels and evaluated as follows [27]:

$$\mathrm{EC} = E\left(log_2\left(det\left(I_N + \frac{\mathrm{SNR}}{N}H\,(H)^H\right)\right)\right)\ \mathrm{bit/s/Hz} \quad (5)$$

where E denotes the averaging operator, I_N denotes the identity matrix of size N, N denotes the number of antennas, SNR denotes the signal-to-noise ratio, and H denotes the channel matrix.

Besides the ergodic capacity, the multiplexing efficiency, η_{mux} which is related to the performance of channel capacity is investigated. The η_{mux} is evaluated using the MIMO antenna performance metrics such as ECC and efficiency, as follows [28]:

$$\eta_{mux} = \sqrt[N]{\left(\prod_{i=1}^{N}\eta_i\right)det\left(\bar{R}\right)} \quad (6)$$

where η_i denotes the i-th antenna efficiency and $det\ (\bar{R})$ denotes the determinant of the matrix of complex envelope correlation. The $\sqrt[N]{\left(\prod_{i=1}^{N}\eta_i\right)}$ describes the geometrical mean of the individual antenna efficiency while $\sqrt[N]{det\left(\bar{R}\right)}$ describes the correlation among the antennas. These two elements provide the impact to improve the η_{mux} which approach to the ideal channel capacity.

The performance of the MIMO antennas is also evaluated using the maximal ratio combining (MRC) technique. The received signals of the multiple antennas are combined using optimal coefficient in this technique. The result is performed in cumulative distribution function (CDF) with the MRC technique and is given as follows [29]:

$$P_{MRC}\ (\gamma \le x) = 1 - \sum_{j=1}^{N}\frac{\lambda_j^{N-1}e^{-SNR/\lambda_j}}{\prod_{k\neq j}^{N}\left(\lambda_j - \lambda_k\right)} \quad (7)$$

where λ_j and λ_k denote the eigenvalues of the SNR covariance matrix at the j-th port and k-th port, respectively.

V. SIMULATION AND EXPERIMENTAL RESULTS

A. S-PARAMETERS

The fabricated prototypes of the optimized PIFAs and CCE antennas with the decoupling network is shown in Fig. 5.

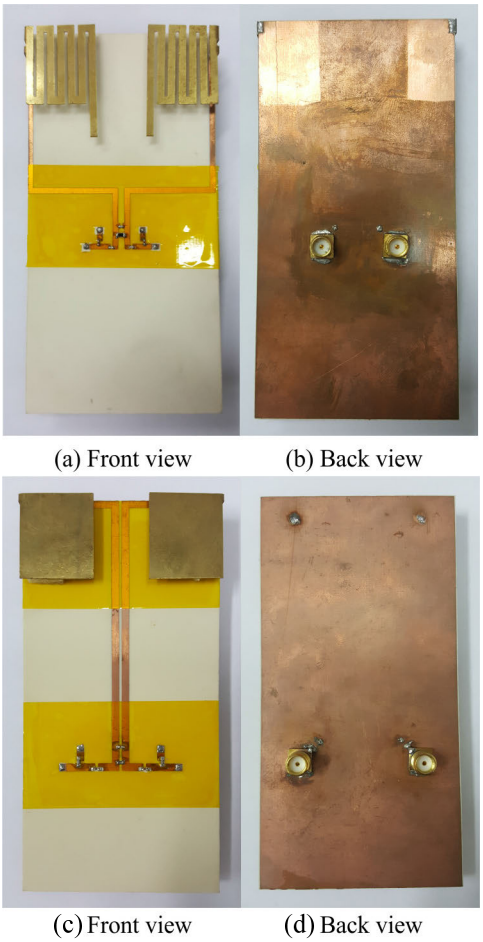

FIGURE 5. Fabricated prototypes of the two-element antennas with the decoupling network: (a) PIFA (front view), (b) PIFA (back view), (c) CCE antennas (front view), and (d) CCE antennas (back view).

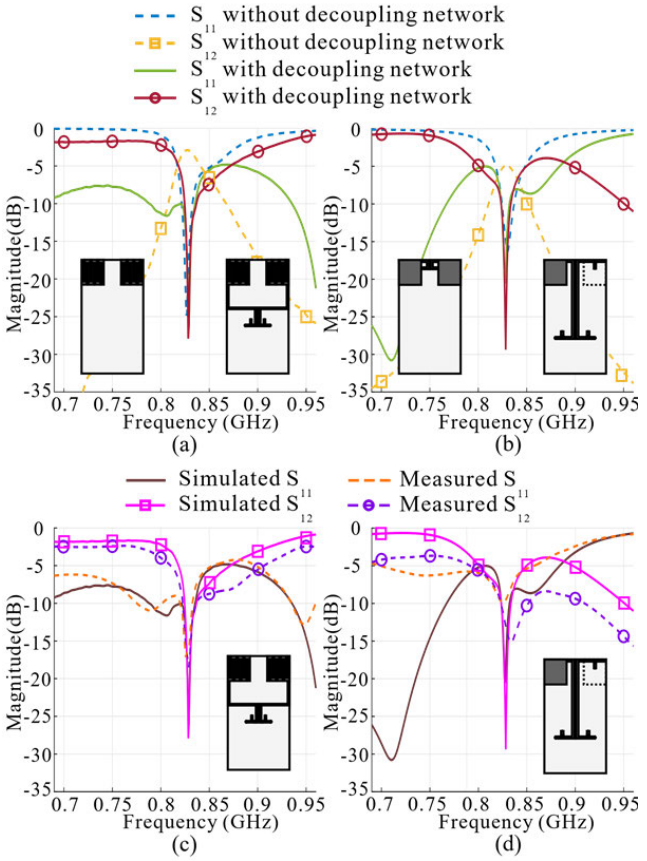

FIGURE 6. (a) Simulated S-parameters of PIFAs with and without the decoupling network. (b) Simulated S-parameters of CCE antennas with and without the decoupling network.; (c) Simulated and measured PIFAs with the decoupling network (d) Simulated and measured CCE antennas with the decoupling network.

The decoupling networks are built using surface mount components for optimized space consumption and minimizing losses.

The simulated and measured S-parameters for both antenna designs are shown in Fig. 6. For the sake of brevity and due to the symmetry of the antenna elements, only S_{11} and S_{12} are shown. The simulated S_{11} and S_{12} values for the PIFAs with and without the decoupling network are first analyzed, and are presented in Fig. 6(a). The designed PIFA without the decoupling network at 0.829 GHz showed S_{11} and S_{12} value of -16 dB and -3 dB, respectively. In comparison, when implemented with the decoupling network, the PIFA, the mutual coupling is reduced significantly from -3 dB to -26 dB. Based on [25] a strong mutual coupling exists when more than one antenna is located in the strong E-field current region. The antennas shared the same E-field excitation at the short edge of the chassis and leads to a high coupling. In this work, it is worth noting that the initial value of mutual coupling determined from the PIFAs and CCE antennas without the decoupling network is above -5 dB. In Fig. 6(a), PIFAs with and without the decoupling network showed a bandwidth of 7.2 MHz (from 0.7881 to 0.8353 GHz) and 11.2 MHz (from 0.8215 to 0.8327 GHz), respectively.

On the other hand, Fig. 6(b) shows the simulated results of the CCE antennas with and without the decoupling network. The CCE antennas with the pre-matching network featured a S_{11} and S_{12} of -16 dB and -5 dB, respectively. When implemented with the decoupling network, the S_{11} and S_{12} is improved to -16 dB and -23 dB, respectively. In Fig. 6(b), the CCE antennas with and without the decoupling network operates from 0.8237 to 0.832 GHz (8.3 MHz) and from

$$\rho_{\mathbf{e}} = \frac{\left|\int_0^{2\pi}\int_0^{\pi}\left(\mathrm{XPR}\,E_{\theta 1}E_{\theta 2}^{*}P_{\theta}+E_{\varphi 1}E_{\varphi 2}^{*}P_{\varphi}\right)\mathrm{d}\Omega\right|^{2}}{\int_0^{2\pi}\int_0^{\pi}\left(\mathrm{XPR}\,E_{\theta 1}E_{\theta 1}^{*}P_{\theta}+E_{\varphi 1}E_{\varphi 1}^{*}P_{\varphi}\right)\mathrm{d}\Omega \times \int_0^{2\pi}\int_0^{\pi}\left(\mathrm{XPR}\,E_{\theta 2}E_{\theta 2}^{*}P_{\theta}+E_{\varphi 2}E_{\varphi 2}^{*}P_{\varphi}\right)\mathrm{d}\Omega} \tag{3}$$

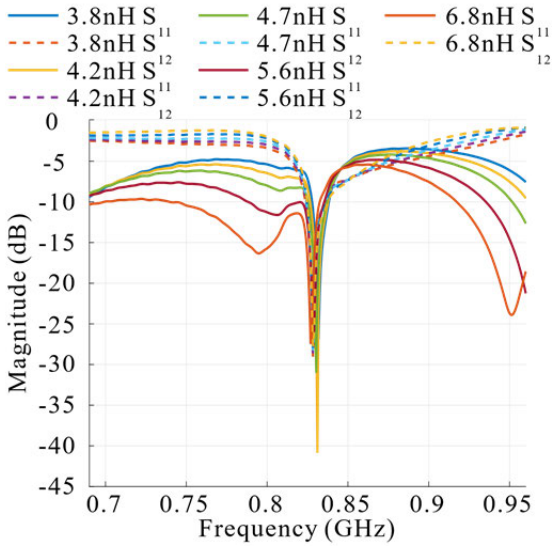

FIGURE 7. Parameter study on inductor values on PIFA matching network.

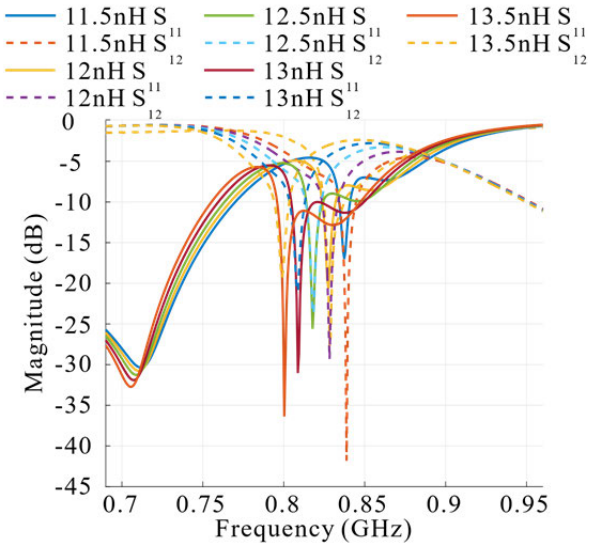

FIGURE 8. Effects of parameter tuning on the CCE pre-matching network.

0.8245 to 0.837 GHz (12.5 MHz), respectively. An important observation is that an additional resonance is found at 0.7 GHz upon the integration with the decoupling network, contributed by the matching circuit. The simulated and measured performance of the PIFA with the decoupling network agreed well, as illustrated in Fig. 6(c). The measured S_{11} and S_{12} at the center frequency are -16 dB and -18 dB, respectively. Meanwhile, the simulated and measured S-parameters of CCE antennas with the decoupling network also agreed well, as depicted in Fig. 6(d). The measured S_{11} and S_{12} of the CCE antennas are -10 dB and -13 dB, respectively. The component values in the three networks (i.e., pre-matching, decoupling, and matching networks) were then optimized for the CCE antennas to eliminate this additional resonance.

B. EFFECT OF MATCHING NETWORK

From Fig. 6(a) and 6(b), the matching bandwidth of the antenna is showing a different behavior. The CCE antennas with the decoupling technique indicated a slight bandwidth decrease and this is aligned with the finding shown in [14] and [30]. On the contrary, the results shown by the PIFA is reversed, which is caused by the additional matching network. This can be seen by observing Fig. 6(a), where an additional resonant frequency resonating slightly lower than 0.829 GHz is introduced when the matching circuit is added. This then broadened the bandwidth of the PIFAs with the decoupling network. To further validate this, additional simulations have been performed. The inductor in the matching network has been tuned from 3.8 nH to 6.8 nH, resulting in the S-parameters shown in Fig. 7. This validates that the existence of the matching network directly influences the bandwidth. This validation can be led to further enhancement of the matching bandwidth after the implementation of the decoupling network on MIMO antennas.

C. EFFECTS OF PRE-MATCHING NETWORK

This section explains the tuning process of the non-resonant antenna element to operate at the target frequency using the pre-matching network. During the tuning process, the CCE antennas are first decoupled with the decoupling. The S-parameters are observed while the inductor in this pre-matching network is tuned from 11.5 nH to 13.5 nH, as shown in Fig. 8. The S-parameters indicate that the operating frequency is lowered with a higher inductor value. Meanwhile, the mutual coupling between the elements remained under -15 dB. This indicates the capability of the CCE antenna in resonating at different frequencies without the need for any modifications to its physical structure. They can potentially can be further miniaturized and integrated with frequency reconfigurable features.

D. MIMO ANTENNA PERFORMANCE

As a final validation of the multiple antennas' performance, it is important to evaluate their MIMO performance in terms of envelope correlation coefficient (ECC), total efficiency and radiation pattern. Fig. 9 shows the ECC values and total efficiency of the multiple antennas with and without the decoupling network. The ECC values are below 0.5 for both PIFAs and CCE antennas at 0.829 GHz, as shown in Fig. 9(a) and 9(c), respectively.

The originally total efficiency of PIFAs and CCE antennas is below 60 %. The total efficiency of the PIFAs and CCE antennas with the proposed decoupling network improved by 30 % and 31 %, as shown in Fig. 9(b) and 9(d), respectively. This also shows that the power loss contributed by the resistors in the decoupling network is small and negligible compared to the contribution of the decoupling network in minimizing the coupling between the two antenna ports. It is worth to mention that it is more challenging to achieve higher total efficiency in the lower Sub-1 GHz band, compared to

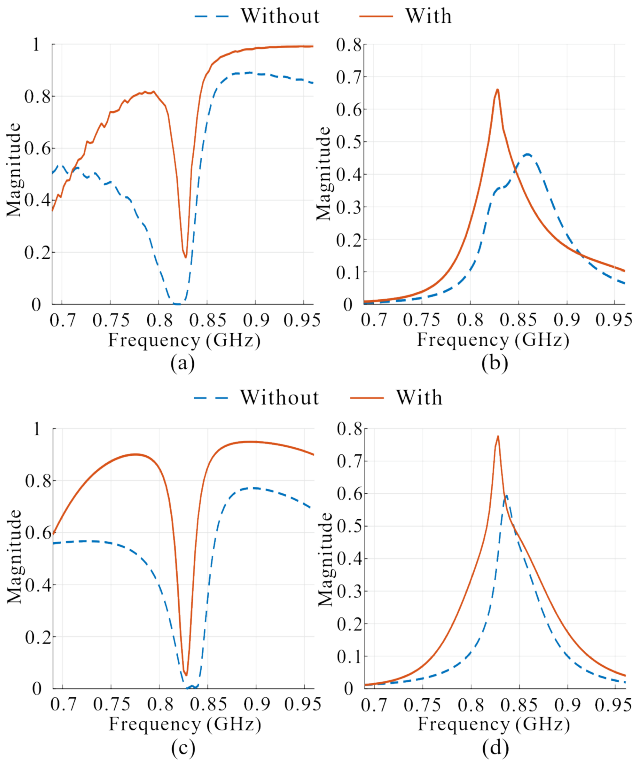

FIGURE 9. Performance of the antennas with and without the decoupling network in terms of: (a) ECC for PIFA, (b) total efficiency for PIFAs, (c) ECC for CCE antennas, (d) total efficiency for CCE antennas.

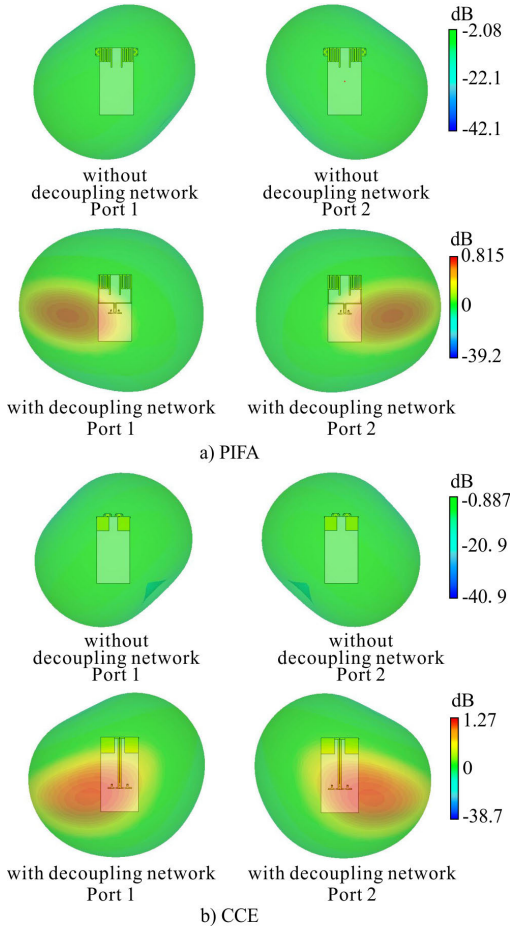

FIGURE 10. Radiation pattern of a) PIFA and b) CCE antennas with and without decoupling network.

higher frequencies above 2 GHz. This is aligned with the finding shown in [31], [32].

Fig. 10 shows the radiation pattern of the PIFAs and CCE antennas with and without the decoupling network. The radiation patterns of port 1 and port 2 for the PIFAs and CCE antennas are quasi-mirror images of each other at 0.829 GHz. From Fig. 10, it is observed that the antennas are radiating toward the Z-direction with an orthogonal behavior when excited from port 1 and port 2, indicating the coverage of complementary space regions in the Z-direction. It can be observed that the realized gain of the antennas without any decoupling techniques is low. Specifically, the realized gain of the PIFAs and CCE antennas are negative in value, at −2.08 dB and −0.887 dB, respectively. The realized gain of these antennas then improved with the implementation of the decoupling network; to 0.815 dB (for the PIFAs) and to 1.27 dB (for the CCE antennas).

It is observed in Fig. 9(a) and 9(c) that the original ECC value is lower than the ECC with the decoupling network. The ECC values before the implementation of the decoupling network is 0.034 (for the PIFA) and 0.001 (for the CCE). These ECC values increased when the antennas are integrated with the decoupling network to 0.18 (for the PIFA) and 0.069 (for the CCE). These values are still under the acceptable ECC limit of 0.5. The main reason for the lower ECC value before decoupling is mainly due to the lower realized gain of the antenna. This is illustrated in the radiation patterns (without the decoupling network) in Fig. 10. Upon the implementation of the decoupling network, the realized gain of the PIFA improved from −2.08 dB to 0.815 dB, resulting in a more directive radiation pattern. The more directive pattern then causes an increase of coupling loss between the antennas, thus slightly increasing the ECC values. Besides that, it can be observed in Figs. 6(a) and 6(b) that the antenna S_{12} are wider before the implementation of the decoupling network. This S_{12} operation which then narrowed with the decoupling network. This same behavior is also seen in Figs. 9(a) and 9(c), as the ECC bandwidth changes with respect to the behavior of S_{12} illustrated in Figs. 6(a) and 6(b). This explains the changes in bandwidth shown by the ECC, and this behavior is aligned with the finding by a recent work [33]. In general, a narrower ECC bandwidth can be expected after the implementation of the decoupling network due to the changes in the S_{12} bandwidth.

The CCE antennas with decoupling network is chosen as the final antenna in this work due to its ease in frequency reconfiguration and further size miniaturization potential. This structure is evaluated further using the ergodic capacity, multiplexing efficiency, and the MRC gain. Fig. 11 shows the ergodic capacity of the CCE antennas with and without the decoupling network, with a 2 x 2 independent and

TABLE 3. Comparison of different antenna elements with decoupling network.

Ref. (year)	Type of Antenna	Frequency	Dimension of antenna	Distance between antennas	IBW	Coupling without decoupling network	Coupling with decoupling network	ECC	Total efficiency	Total Efficiency Improvement
[12] (2020)	Slot	3.3 – 3.7 GHz	22.5 x 1.5 mm^2 (0.491 λ_g x 0.033 λ_g)	0.58 λ_g	7 %	-9 dB	-25 dB	< 0.04	85 %	10 %
[13] (2017)	Monopole	2.45 GHz	21.5 x 1.5 mm^2 (0.360 λ_g x 0.025 λ_g)	0.14 λ_g	8.8 %	-2.5 dB	-20.1 dB	-	72 %	10 %
[14] (2017)	Monopole	0.74 GHz	38 x 11 mm^2 (0.501 λ_g x 0.054 λ_g)	0.23 λ_g	2.2 %	-6 dB	-25 dB	< 0.03	67 %	9 %
[15] (2016)	Monopole	2.45 GHz	25.1 x 2.5 mm^2 (0.429 λ_g x 0.042 λ_g)	0.157 λ_g	4%	-4 dB	-24.5 dB	< 0.2	61.6 %	16.7 %
[17] (2019)	Monopole	2.4 GHz	50 x 56 mm^2 (0.765 λ_g x 0.857 λ_g)	0.131 λ_g	2.9 %	-8 dB	-25dB	<0.1	72.5 %	21 %
This work	PIFA	0.829 GHz	20 x 23 mm^2 (0.101 λ_g x 0.116 λ_g)	0.076 λ_g	5.8%	-3 dB	-26 dB	< 0.2	65.69 %	30 %
	CCE				1%	-5 dB	-23 dB	< 0.2	75.48 %	31 %

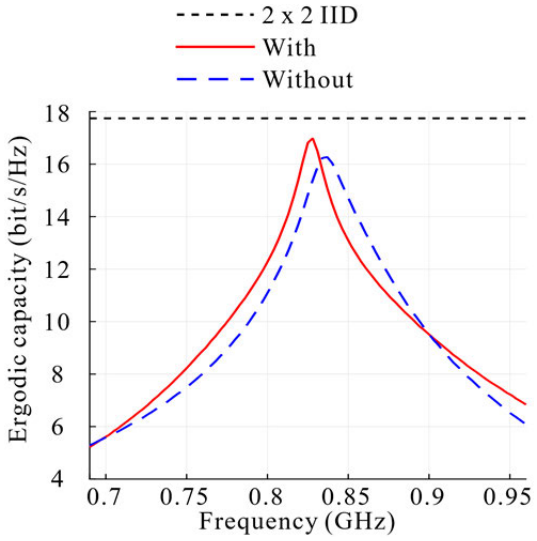

FIGURE 11. Ergodic capacity of the CCE antennas in free space with and without the decoupling network, and a 2 x 2 IID capacity.

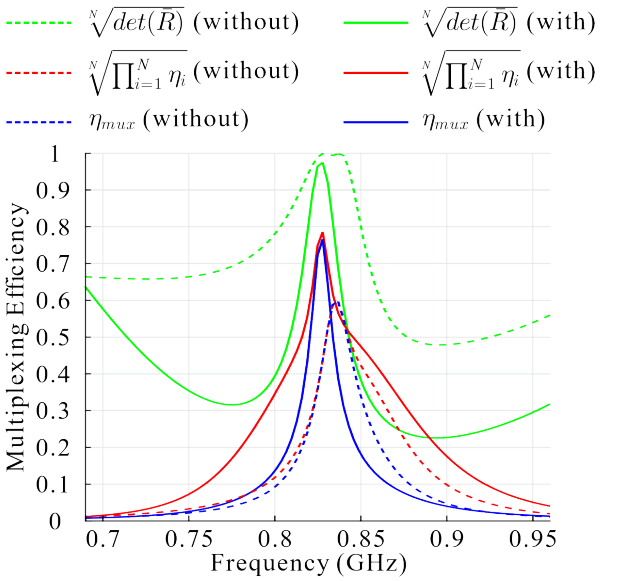

FIGURE 12. Multiplexing efficiency of the CCE antennas with and without the decoupling network in free space.

identically distributed (IID) capacity as reference. The number of the random channel realization is fixed at 50,000 to ensure the satisfactory accuracy, whereas the ergodic capacity is calculated at an SNR value of 20 dB. In free space, the ergodic capacity at 0.829 GHz is improved from 15.39 to 16.99 bit/s/Hz, and is closer to the IID capacity of 17.75 bit/s/Hz.

Fig. 12 depicts the multiplexing efficiency (η_{mux}) for the CCE antennas with the decoupling network in free space. It improved the η_{mux} by 0.329, from 0.437 to 0.766. Besides this, the contributions of the elements to the η_{mux} results (i.e., $\sqrt[N]{\left(\prod_{i=1}^{N}\eta_i\right)}$ and $\sqrt[N]{det\left(\bar{R}\right)}$ from equation (5)) are provided in Fig. 12. It can be observed η_{mux} is mainly influenced by the $\sqrt[N]{\left(\prod_{i=1}^{N}\eta_i\right)}$ term. On the contrary, the term $\sqrt[N]{det\left(\bar{R}\right)}$ remained consistent, with a close-to-unity value with and without the decoupling network.

Fig. 13 shows the CDF curves of the MRC gain (scaled from 0 to 1) for the CCE antennas in free space. The effects of the decoupling network to the individual antenna at 0.829 GHz can be observed when the CDF curves are shifted to the higher normalized SNR values. The MRC diversity gain is illustrated in this figure using the MRC gain. The highest MRC gain of the individual antenna is at a CDF level of 0.5. The MRC diversity gain of the CCE antennas with and without the decoupling network are 3.769 dB and 3.618 dB, respectively.

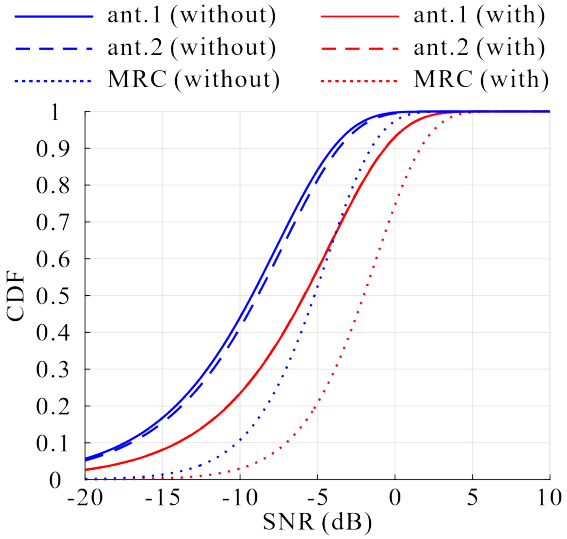

FIGURE 13. CDF of the MRC gain and the individual CCE antennas with and without the decoupling network in free space.

Table 3 compares the antenna performance with the proposed decoupling network with other relevant antennas available in literature. The distance between antennas in all literature are less than the conventional requirement of a quarter wavelength except for [12]. It is evident that the antennas with the decoupling network proposed are capable to be spaced with the smallest inter-element distance of 0.08 λ_g. In addition to that, the PIFAs and CCE antennas featured better performance in terms of total efficiency, with at least 13.3 % of improvement relative to other published works. At the same time, the levels of coupling level reduction offered by this work are comparable, if not better than these literatures, which have been mainly designed for operation in the 2.4 GHz band.

VI. CONCLUSION

In this work, a decoupling network applicable for a two-element PIFA and CCE antenna in a compact mobile terminal are presented for Sub-1 GHz band. Both proposed multiple antennas are designed to operate in the same frequency band and similarly dimensioned to provide a fair comparison. Results in terms of S-parameters, ECC, and total efficiency indicated that this decoupling network can be implement on different resonant and non-resonant antenna elements with improved inter-element distance (of up to 34 % nearer) and total efficiency improvements (of up to 30 %) at the same time. These features are especially advantageous for mobile terminals with multiple CCE antennas in the Sub-1 GHz frequency bands. In addition, further investigation of CCE antennas with decoupling network shown promising enhancement in terms of ergodic capacity, multiplexing efficiency, and MRC diversity gain. Moreover, additional antenna miniaturization can be further implemented by optimization of the pre-matching network, decoupling network, and matching network. Finally, a tunable decoupling network on multiple antennas is planned for future work.

REFERENCES

[1] Q. Sun, B. Sun, L. Sun, W. Huang, and Q. Ren, "Broadband two-element array with hybrid decoupling structures for multimode mobile terminals," *IEEE Antennas Wireless Propag. Lett.*, vol. 14, pp. 1431–1434, 2015.

[2] A. C. K. Mak, C. R. Rowell, and R. D. Murch, "Isolation enhancement between two closely packed antennas," *IEEE Trans. Antennas Propag.*, vol. 56, no. 11, pp. 3411–3419, Nov. 2008.

[3] B. K. Lau and J. B. Andersen, "Simple and efficient decoupling of compact arrays with parasitic scatterers," *IEEE Trans. Antennas Propag.*, vol. 60, no. 2, pp. 464–472, Feb. 2012.

[4] A. Cihangir, F. Ferrero, G. Jacquemod, P. Brachat, and C. Luxey, "Neutralized coupling elements for MIMO operation in 4G mobile terminals," *IEEE Antennas Wireless Propag. Lett.*, vol. 13, pp. 141–144, 2014.

[5] H.-J. Chen, T.-H. Huang, C.-S. Chang, L.-S. Chen, N.-F. Wang, Y.-H. Wang, and M.-P. Houng, "A novel cross-shape DGS applied to design ultra-wide stopband low-pass filters," *IEEE Microw. Wireless Compon. Lett.*, vol. 16, no. 5, pp. 252–254, May 2006.

[6] X. Zhao, S. P. Yeo, and L. C. Ong, "Planar UWB MIMO antenna with pattern diversity and isolation improvement for mobile platform based on the theory of characteristic modes," *IEEE Trans. Antennas Propag.*, vol. 66, no. 1, pp. 420–425, Jan. 2018.

[7] F. Yang and Y. Rahmat-Samii, "Microstrip antennas integrated with electromagnetic band-gap (EBG) structures: A low mutual coupling design for array applications," *IEEE Trans. Antennas Propag.*, vol. 51, no. 10, pp. 2936–2946, Oct. 2003.

[8] S. Zhang, X. Chen, and G. F. Pedersen, "Mutual coupling suppression with decoupling ground for massive MIMO antenna arrays," *IEEE Trans. Veh. Technol.*, vol. 68, no. 8, pp. 7273–7282, Aug. 2019.

[9] L. Zhao, F. Liu, X. Shen, G. Jing, Y.-M. Cai, and Y. Li, "A high-pass antenna interference cancellation chip for mutual coupling reduction of antennas in contiguous frequency bands," *IEEE Access*, vol. 6, pp. 38097–38105, 2018.

[10] B. C. Pan and T. J. Cui, "Broadband decoupling network for dual-band microstrip patch antennas," *IEEE Trans. Antennas Propag.*, vol. 65, no. 10, pp. 5595–5598, Oct. 2017.

[11] L. Zhao, L. K. Yeung, and K.-L. Wu, "A coupled resonator decoupling network for two-element compact antenna arrays in mobile terminals," *IEEE Trans. Antennas Propag.*, vol. 62, no. 5, pp. 2767–2776, May 2014.

[12] Y.-F. Cheng and K.-K.-M. Cheng, "Compact wideband decoupling and matching network design for dual-antenna array," *IEEE Antennas Wireless Propag. Lett.*, vol. 19, no. 5, pp. 791–795, May 2020.

[13] S. N. Venkatasubramanian, L. Li, A. Lehtovuori, C. Icheln, and K. Haneda, "Impact of using resistive elements for wideband isolation improvement," *IEEE Trans. Antennas Propag.*, vol. 65, no. 1, pp. 52–62, Jan. 2017.

[14] H. Meng and K. Wu, "An LC decoupling network for two antennas working at low frequencies," *IEEE Antennas Wireless Propag. Lett.*, vol. 65, no. 7, pp. 2321–2329, Jul. 2017.

[15] C.-H. Wu, C.-L. Chiu, and T.-G. Ma, "Very compact fully lumped decoupling network for a coupled two-element array," *IEEE Antennas Wireless Propag. Lett.*, vol. 15, pp. 158–161, 2016.

[16] S.-C. Chen, Y.-S. Wang, and S.-J. Chung, "A decoupling technique for increasing the port isolation between two strongly coupled antennas," *IEEE Trans. Antennas Propag.*, vol. 56, no. 12, pp. 3650–3658, Dec. 2008.

[17] M. Li, L. Jiang, and K. L. Yeung, "Novel and efficient parasitic decoupling network for closely coupled antennas," *IEEE Trans. Antennas Propag.*, vol. 67, no. 6, pp. 3574–3585, Jun. 2019.

[18] Y.-L. Ban, Y.-F. Qiang, Z. Chen, K. Kang, and J. L.-W. Li, "Low-profile narrow-frame antenna for seven-band WWAN/LTE smartphone applications," *IEEE Antennas Wireless Propag. Lett.*, vol. 13, pp. 463–466, 2014.

[19] R. Valkonen, J. Ilvonen, C. Icheln, and P. Vainikainen, "Inherently non-resonant multi-band mobile terminal antenna," *Electron. Lett.*, vol. 49, no. 1, pp. 11–13, Jan. 2013.

[20] X. Lei and S. H. Rhee, "Performance improvement of sub 1 GHz WLANs for future IoT environments," *Wireless Pers. Commun.*, vol. 93, no. 4, pp. 933–947, Apr. 2017.

[21] J. A. Tirado-Mendez, R. Acevo-Herrera, R. Flores-Leal, R. Linares-Miranda, and H. Jardon-Aguilar, "IFA and PIFA size reduction by using a stub loading," *Int. J. Antennas Propag.*, vol. 2013, pp. 1–7, Nov. 2013.

[22] J. Holopainen, R. Valkonen, O. Kivekas, J. Ilvonen, and P. Vainikainen, "Broadband equivalent circuit model for capacitive coupling element–based mobile terminal antenna," *IEEE Antennas Wireless Propag. Lett.*, vol. 9, pp. 716–719, 2010.

[23] H. Li, Y. Tan, B. K. Lau, Z. Ying, and S. He, "Characteristic mode based tradeoff analysis of antenna-chassis interactions for multiple antenna terminals," *IEEE Trans. Antennas Propag.*, vol. 60, no. 2, pp. 490–502, Feb. 2012.
[24] S.-C. Chen, L.-C. Chou, C.-I.-G. Hsu, and S.-M. Li, "Compact sub-6-GHz four-element MIMO slot antenna system for 5G tablet devices," *IEEE Access*, vol. 8, pp. 154652–154662, 2020.
[25] S. Zhang, K. Zhao, Z. Ying, and S. He, "Investigation of diagonal antenna-chassis mode in mobile terminal LTE MIMO antennas for bandwidth enhancement," *IEEE Antennas Propag. Mag.*, vol. 57, no. 2, pp. 217–228, Apr. 2015.
[26] X. Chen, S. Zhang, and Q. Li, "A review of mutual coupling in MIMO systems," *IEEE Access*, vol. 6, pp. 24706–24719, 2018.
[27] M. S. Sharawi, A. T. Hassan, and M. U. Khan, "Correlation coefficient calculations for MIMO antenna systems: A comparative study," *Int. J. Microw. Wireless Technol.*, vol. 9, no. 10, pp. 1991–2004, Dec. 2017.
[28] R. Tian, B. K. Lau, and Z. Ying, "Multiplexing efficiency of MIMO antennas," *IEEE Antennas Wireless Propag. Lett.*, vol. 10, pp. 183–186, 2011.
[29] V. Papamichael, M. Karaboikis, C. Soras, and V. Makios, "Diversity and MIMO performance evaluation of common phase center multi element antenna systems," *Radioengineering*, vol. 17, no. 2, p. 33, 2008.
[30] Z. Wang, L. Zhao, Y. Cai, S. Zheng, and Y. Yin, "A meta-surface antenna array decoupling (MAAD) method for mutual coupling reduction in a MIMO antenna system," *Sci. Rep.*, vol. 8, no. 1, pp. 1–9, Feb. 2018.
[31] C. S. Young, "Noise, interference, and emanations," in *Information Security Science*. Amsterdam, The Netherlands: Syngress, 2016, ch. 5, pp. 103–122.
[32] L. H. Trinh, F. Ferrero, L. Lizzi, R. Staraj, and J.-M. Ribero, "Reconfigurable antenna for future spectrum reallocations in 5G communications," *IEEE Antennas Wireless Propag. Lett.*, vol. 15, pp. 1297–1300, 2016.
[33] J. Li, X. Zhang, Z. Wang, X. Chen, J. Chen, Y. Li, and A. Zhang, "Dual-band eight-antenna array design for MIMO applications in 5G mobile terminals," *IEEE Access*, vol. 7, pp. 71636–71644, 2019.

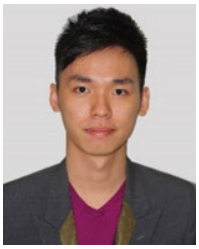

WAI LOON CHEOR (Graduate Student Member, IEEE) was born in Perak, Malaysia. He received the B.Eng. degree in communication engineering from Universiti Malaysia Perlis (UniMAP), Malaysia, in 2014, where he is currently pursuing the Ph.D. degree in communication engineering. His current research interests include multi-element antennas and mobile terminal antennas.

AZREMI ABDULLAH AL-HADI (Senior Member, IEEE) was born in Michigan, USA, in August 26. He received the M.Sc. degree in communication engineering from the University of Birmingham, U.K., in 2004, and the D.Sc. degree in technology from Aalto University, Finland, in 2013.

He is currently working as an Associate Professor and holds a position as the dean of the Faculty of Electronic Engineering Technology, Universiti Malaysia Perlis (UniMAP), where he has been with the School of Computer and Communication Engineering, since 2002. His current research interests include design and performance evaluation of multielement antennas, mobile terminal antennas and their user interactions, and wireless propagation.

Dr. Al-Hadi is also a Chartered Engineer of the Institution of Engineering and Technology (IET), U.K., a member of the Board of Engineers Malaysia (BEM), Malaysia, and a Graduate Technologist of the Malaysia Board of Technologist (MBOT), Malaysia. He was a recipient of the Best Student Paper Award presented at the Fifth Loughborough Antennas and Propagation Conference (LAPC 2009) and the CST University Publication Award, in 2011. He is also active in volunteering work with the IEEE Malaysia Section, acting as the Vice Chair of the IEEE Antenna Propagation / Microwave Theory Techniques / Electromagnetic Compatibility (AP/MTT/EMC) Malaysia Chapter, and the Counselor of the IEEE UniMAP Student Branch.

PING JACK SOH (Senior Member, IEEE) was born in Sabah, Malaysia. He received the B.Eng. and M.Eng. degrees from Universiti Teknologi Malaysia and the Ph.D. degree from the ESAT-TELEMIC Research Division, KU Leuven, Belgium.

He is currently an Associate Professor with the Faculty of Electronic Engineering Technology, Universiti Malaysia Perlis (UniMAP), and a Research Affiliate with KU Leuven. From 2002 to 2004, he was a Test Engineer with Venture Corporation. In 2005, he joined Motorola Solutions Malaysia, as a Research and Development Engineer. Since 2006, he has been a Lecturer with UniMAP before pursuing the Ph.D. degree with the ESAT-TELEMIC Research Division, KU Leuven, as a Research Assistant, from 2009 to 2013, and then a Postdoctoral Fellow, from 2013 to 2014. His research interests include wearable antennas, flexible antennas/metasurfaces, electromagnetic safety and absorption, and wireless techniques for healthcare applications. He is also a Chartered Engineer of the U.K. Engineering Council, a Professional Technologist with the Malaysia Board of Technologists (MBOT), and a member of the IET and URSI. He was a recipient of the URSI Young Scientist Award, in 2015, the IEEE MTT-S Graduate Fellowship for Medical Applications, in 2013, and the IEEE AP-S Doctoral Research Award, in 2012. He was also the Second Place Winner of the IEEE Presidents' Change the World Competition, in 2013. He also serves on the IEEE MTT-S Education Committee.

MOHD FAIZAL JAMLOS (Senior Member, IEEE) received the M.Sc. degree from the University of Adelaide, South Australia, Australia, in 2008, and the Ph.D. degree from Universiti Teknologi Malaysia, Johor, Malaysia, in 2010. He is currently a Professor with the Faculty of Mechanical Engineering, Universiti Malaysia Pahang (UMP). Previously he was an Associate Professor with the Advanced Communication Engineering Centre (ACE), School of Computer and Communication Engineering, Universiti Malaysia Perlis. He has coauthored more than 220 scientific publications in peer-reviewed journals and conferences. His research interests include wireless embedded systems, remote sensing, on-platform antennas and microwave circuitry, and the IoT applications. He is also a Practice Professional Engineer of Board of Engineers Malaysia (BEM), a National Medical Researcher (NMRR) and a Corporate Member of the Institute Engineers Malaysia (MIEM).

AHMED MOHAMED ELSHIRKASI received the M.Sc. degree in communication engineering from International Islamic University Malaysia (IIUM), in 2015. He is currently pursuing the Ph.D. degree with Universiti Malaysia Perlis (UniMAP). His current research interests include the performance evaluation of multielement antennas, mobile terminal antennas and their user interactions, and wireless propagation.

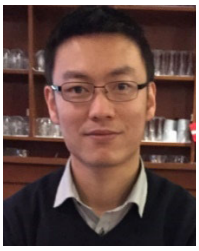

XIAOMING CHEN (Senior Member, IEEE) received the B.Sc. degree in electrical engineering from Northwestern Polytechnical University, Xi'an, China, in 2006, and the M.Sc. and Ph.D. degrees in electrical engineering from the Chalmers University of Technology, Gothenburg, Sweden, in 2007 and 2012, respectively.

From 2013 to 2014, he was a Postdoctoral Researcher with the Chalmers University of Technology. From 2014 to 2017, he was with Qamcom Research and Technology AB, Gothenburg, where he was involved in the EU H2020 5GPPP mmMAGIC Project (working on 5G millimeter-Wave wireless access techniques). Since 2017, he has been a Professor with Xi'an Jiaotong University, Xi'an. He has coauthored one book, one book chapter, more than 60 journal articles, and over 60 conference papers on his research topics. His research interests include 5G multiantenna techniques, over-the-air (OTA) testing, reverberation chambers, and hardware impairments and mitigation. He received the International Union of Radio Science (URSI) Young Scientist Awards, in 2017 and 2018. He received the outstanding AE awards, in 2018 and 2019. He was a Guest Editor of the of the journal of *IET Microwaves, Antennas and Propagation* Special Issue on Metrology for 5G Technologies. He serves as an Associate Editor (AE) for the journal of IEEE Antennas and Wireless Propagation Letters.

PRAYOOT AKKARAEKTHALIN (Member, IEEE) received the B.Eng. and M.Eng. degrees in electrical engineering from the King Mongkut's University of Technology North Bangkok (KMUTNB), Bangkok, Thailand, in 1986 and 1990, respectively, and the Ph.D. degree from the University of Delaware, Newark, DE, USA, in 1998. From 1986 to 1988, he was a Research and Development Engineer with Microtek Company Ltd., Thailand. In 1988, he joined the Department of Electrical Engineering, KMUTNB. He has authored or coauthored over 40 international journals, more than 200 conference papers, and four books/book chapters. His current research interests include RF/microwave circuits, wideband and multiband antennas, telecommunications, and sensor systems. He is currently a member of the IEICE Japan, ECTI, and EEAAT Associations Thailand. He was the Chairman of the IEEE MTT/AP/ED Thailand Joint Chapter, from 2007 to 2010, and the Vice President and the President of the ECTI Association, Thailand, from 2012 to 2013 and from 2014 to 2015, respectively. He is also the Leader of TRF Senior Research Scholar Project of "Innovative Sensor Technology for Thailand Development" granted by the Thailand Research Fund, Thailand. He was the Editor-in-Chief for the *ECTI Transactions*, from 2011 to 2013.